

X-Ray and Neutron Reflectivity for the Investigation of Thin Films

– A Short Tutorial –

Frank Schreiber, Alexander Gerlach,
Bereich für Physik der molekularen und biologischen Materie,
Institut für Angewandte Physik, Universität Tübingen,
Auf der Morgenstelle 10, 72076 Tübingen, Germany
www.soft-matter.uni-tuebingen.de

In this tutorial, we give an introduction to the principles of X-ray and neutron reflectivity. For applications of X-ray and neutron reflectivity to organic thin films, see [1,2]. For further technical details see the list of references.

1 Optical Effects at the Interface

When an X-ray beam impinges on the surface of a sample, similar considerations apply as for optics with visible light, i.e. the index of refraction n is the relevant parameter. For X-rays, i.e. electromagnetic radiation with a wavelength λ around 1 Å, we find [1,3,4]

$$n = 1 - \delta + i\beta \quad (1)$$

with

$$\delta = \frac{\lambda^2}{2\pi} r_e \rho_e \quad (2)$$

and

$$\beta = \frac{\lambda}{4\pi} \mu_x. \quad (3)$$

$r_e = 2.818 \times 10^{-15} \text{m}$ is the classical electron radius, ρ_e is the electron density of the material, and μ_x is the absorption length. With $\delta > 0$ we find that $n < 1$, which leads to the phenomenon of so-called total external reflection for incident angles α_i below the critical angle $\alpha_c = \sqrt{2\delta}$.

Typical values for δ are $10^{-5} \dots 10^{-6}$, and thus α_c is in the range of $0.1^\circ \dots 0.5^\circ$. For simplicity, β , which is usually even smaller, will be ignored here. Our considerations apply irrespective of the atomic-scale structure of the material and only the average electron density enters the equations.

We note that an analogous description of the index of refraction applies to the case of neutrons, namely

$$\delta = \frac{\lambda^2}{2\pi} b \rho_n \quad \text{and} \quad \beta = \frac{\lambda}{4\pi} \mu_n. \quad (4)$$

Generally, the order of magnitude for δ and β is similar to the X-ray case. However, since the scattering length b of the nuclei varies non-monotonously across the periodic table, as opposed to the case of X-rays, the contrast between two given elements is different for X-rays and for neutrons. Thus, X-ray and neutron reflectivity can be used in a complementary fashion. Moreover, for neutrons a contrast even between different isotopes of one and the same chemical element can be obtained. The most famous example is the large difference in b between ^1H and ^2D , i.e. hydrogen with protons or deuterons as nuclei. Since hydrogen is ubiquitous in organic matter, deuteration is a frequently applied method to obtain contrast between different organic materials, which for X-rays, i.e. in terms of their electron densities, have very little or no contrast [5].

2 Reflectivity

We discuss the reflectivity for various experimental situations and how it is analyzed. With the exception of Sec. 2.4, we are only concerned with the specular part, i.e. the incident angle α_i and exit angle α_f are equal. In this case the momentum transfer $\vec{Q} = \vec{k}_f - \vec{k}_i$ is along the surface normal, which is chosen to be the z coordinate ($\vec{Q} = Q_z \vec{e}_z$). For a given wavelength λ momentum transfer is derived to be

$$Q_z = \frac{4\pi}{\lambda} \sin \alpha_i \quad (5)$$

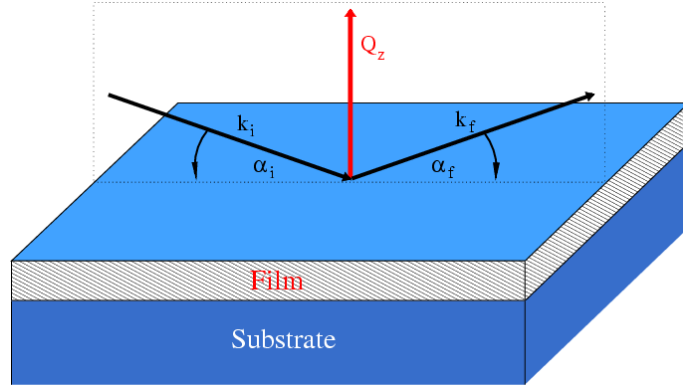


Figure 1: Geometry for specular reflectivity. The initial and the final wave vector \vec{k}_i and \vec{k}_f define the scattering plane.

2.1 Ideal Surface: FRESNEL-Reflectivity

The complex reflection coefficient of the electrical field for an ideal, sharp interface as first calculated by FRESNEL writes [1]

$$r = \frac{k_z - k'_z}{k_z + k'_z}. \quad (6)$$

The reflected intensity is then $R_F = |r|^2$. k_z and k'_z are the vertical component of, respectively, the incident and transmitted wave.

Close to the critical angle k'_z is strongly affected by refraction effects. We find

$$k'_z = k\sqrt{\alpha_i - \alpha_c} \quad (7)$$

which means that for $\alpha_i < \alpha_c$ it is purely imaginary

$$k'_z = ik\sqrt{\alpha_c - \alpha_i}. \quad (8)$$

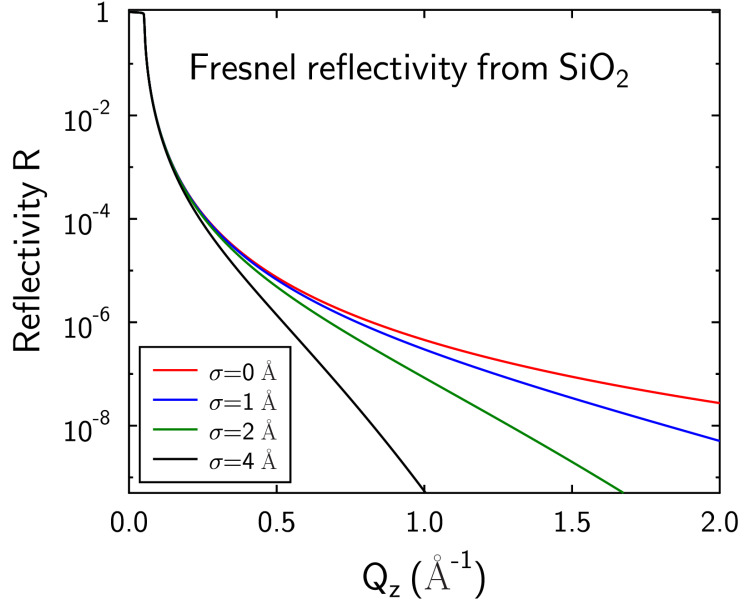


Figure 2: Specular FRESNEL-reflectivity from SiO₂ surface with different roughnesses σ according to equation (9).

Above the critical angle, where k'_z is not very different from k_z , the reflected intensity falls off rapidly ($R_F \propto 1/\alpha_i^4$). Uncorrelated surface roughness σ may be included by

$$r_{rough} = r_{ideal} e^{-2k_z k'_z \sigma^2}. \quad (9)$$

A classical example is the reflectivity from the surface of water, for which deviations from $R_F(\alpha_i)$ can be traced to thermally excited capillary waves, which always lead to a finite roughness [6].

2.2 Multiple Interfaces: PARRATT-Formalism

If the sample has more than one interface (e.g., like a film on a substrate), the scattering from all interfaces has to be taken into account. PARRATT developed a recursion formalism [7], which relates the reflected and transmitted amplitude, R_j and T_j , respectively, via [1]

$$X_j = \frac{R_j}{T_j} = e^{-2ik_z z_j} \frac{r_{j,j+1} + X_{j+1} e^{2ik_z z_{j+1}}}{1 + r_{j,j+1} X_{j+1} e^{2ik_z z_{j+1}}}, \quad (10)$$

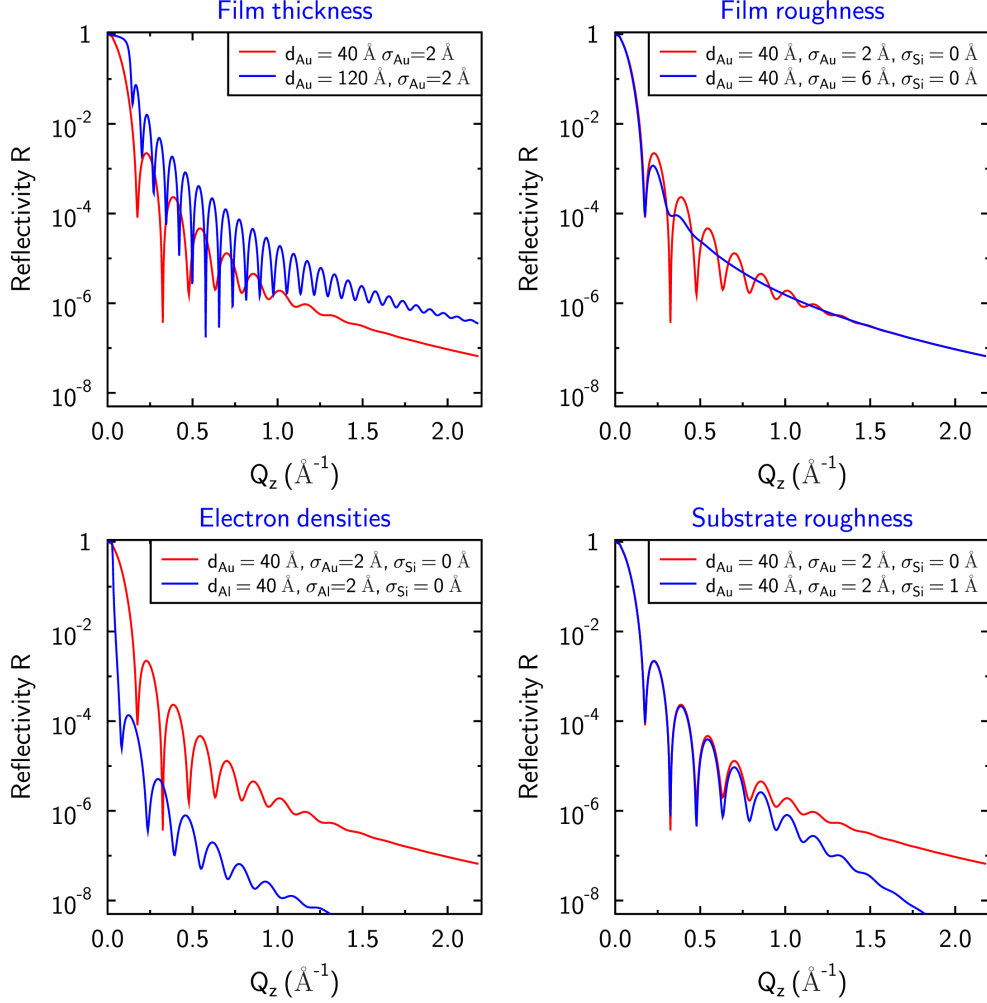


Figure 3: Reflectivity from different films on Silicon according to PARRATs algorithm. The details of the KIESSIG-fringes depend on the film thickness, film roughness, electron density, and substrate roughness.

where

$$r_{j,j+1} = \frac{k_{z,j} - k_{z,j+1}}{k_{z,j} + k_{z,j+1}} \quad (11)$$

is the FRESNEL coefficient of interface j . The recursion is solved using $T_1 = 1$ (incident wave normalized to unity) and $R_{N+1} = 0$ (no reflection from the substrate, i.e., from below the substrate surface).

Due to the interference of waves, which are reflected from different interfaces within a system, intensity oscillations in the reflectivity can be observed. The periodicity in Q_z of these so-called KIESSIG-fringes can be related to the thickness d of the film via $2\pi/d$. Roughness of the interfaces can be taken into account in the same fashion as above, i.e. by including a term $e^{-2k_{z,j}k_{z,j+1}\sigma_{j,j+1}^2}$ in the FRESNEL coefficients, provided that the roughnesses are small compared to thicknesses of the layers involved. We should note that the PARRATT formalism takes into account multiple scattering effects, i.e. it is “dynamical”.

2.3 The Master-Formula

For $\alpha_i \gg \alpha_c$, using kinematical approximation, the reflectivity of an arbitrary electron density profile $\rho_e(z)$ can be described by the so-called “Master-Formula”

$$R(Q_z) = R_F \left| \frac{1}{\rho_e(z \rightarrow \infty)} \int \frac{d\rho_e}{dz} e^{iQ_z z} dz \right|^2. \quad (12)$$

While this formalism in general does not properly take into account the effects around the critical angle, it is fairly good for higher angles and has the important advantage of a closed-form equation. It is also very transparent in that it relates the scattering to spatial changes in the electron density, i.e. only points with non-zero $d\rho/dz$ contribute to the Fourier transform.

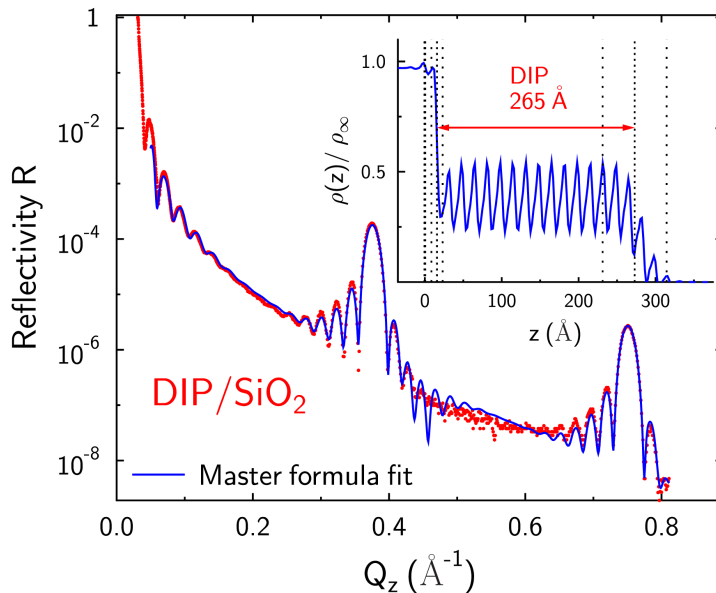


Figure 4: Fit to experimental reflectivity data using the Master-Formula

An example of the structural and thermal analysis of organic light-emitting materials using this straight-forward formalism can be found in Ref. [8]. Another useful application of the master-formula is for graded interfaces [4]. For a systematic investigation of deviations of the “Master-formula” from the more elaborate PARRATT formalism and various other approximations, see Ref. [9].

2.4 Rough Surfaces: Diffuse Scattering

As shown above, interface roughness reduces the specularly reflected intensity. The missing intensity is scattered into other (non-specular) directions. Whereas the specular reflectivity is only sensitive to the structure projected to the surface normal, i.e. the electron density profile $\rho_e(z)$, the non-specularly reflected (i.e. diffuse) intensity is sensitive to the in-plane correlations of the interface, since it has a non-zero component of the momentum transfer in the plane.

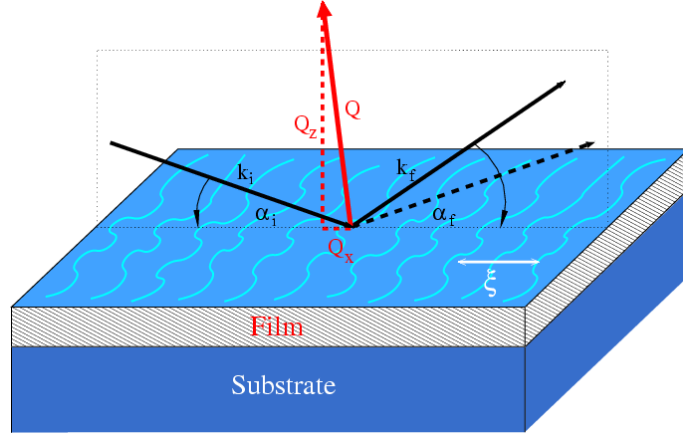


Figure 5: Geometry for non-specular reflectivity

For a statistically meaningful description of the surface, it is customary to introduce the height-difference function

$$g(\vec{r}) = \langle [h(\vec{r}') - h(\vec{r}'')]^2 \rangle \quad (13)$$

and the height-height correlation function

$$C(\vec{r}) = \langle h(\vec{r}')h(\vec{r}'') \rangle \quad (14)$$

which are related via

$$g(r) = 2\sigma^2 - 2C(r). \quad (15)$$

$\vec{r} = \vec{r}' - \vec{r}''$ is a difference coordinate in the plane of the surface, which we assume to be isotropic. $\langle \dots \rangle$ denotes the average over the entire surface. $C(r)$ can be parametrized in various ways. A very flexible form is

$$C(r) = \sigma^2 e^{-(r/\xi)^{2H}} \quad (16)$$

which yields for the limiting cases

$$\lim_{r \rightarrow \infty} C(r) = 0 \quad \text{and} \quad \lim_{r \ll \xi} C(r) = \sigma^2 - \frac{1}{2} r^{2H}. \quad (17)$$

ξ is a typical length scale for the correlations in the plane, and H is the so-called Hurst parameter. For $H \ll 1$ the surface is very “jagged”, whereas for $H \rightarrow 1$ it is varying more smoothly.

Sinha et al. have shown how to relate the lateral correlations to the diffuse scattering [10]. In the kinematical approximation, i.e. sufficiently far away from α_c , it can be written as

$$I_{diffuse} = \frac{\Delta\rho_e}{Q_z^2} e^{-Q_z^2\sigma^2} \int [e^{Q_z^2 C(r)} - 1] e^{i\vec{Q}_{\parallel} \cdot \vec{r}} d\vec{r}. \quad (18)$$

For $Q_z^2 C(r) \ll 1$, i.e. for small roughnesses, the integrand can be expanded and further simplified to yield

$$I_{diffuse} = \Delta\rho_e e^{-Q_z^2\sigma^2} \int C(r) e^{i\vec{Q}_{\parallel} \cdot \vec{r}} d\vec{r}. \quad (19)$$

In this limit the diffuse scattering corresponds directly to the Fourier transform of the height-height correlation function $C(r)$. For a more detailed discussion, see Ref. [1, 3].

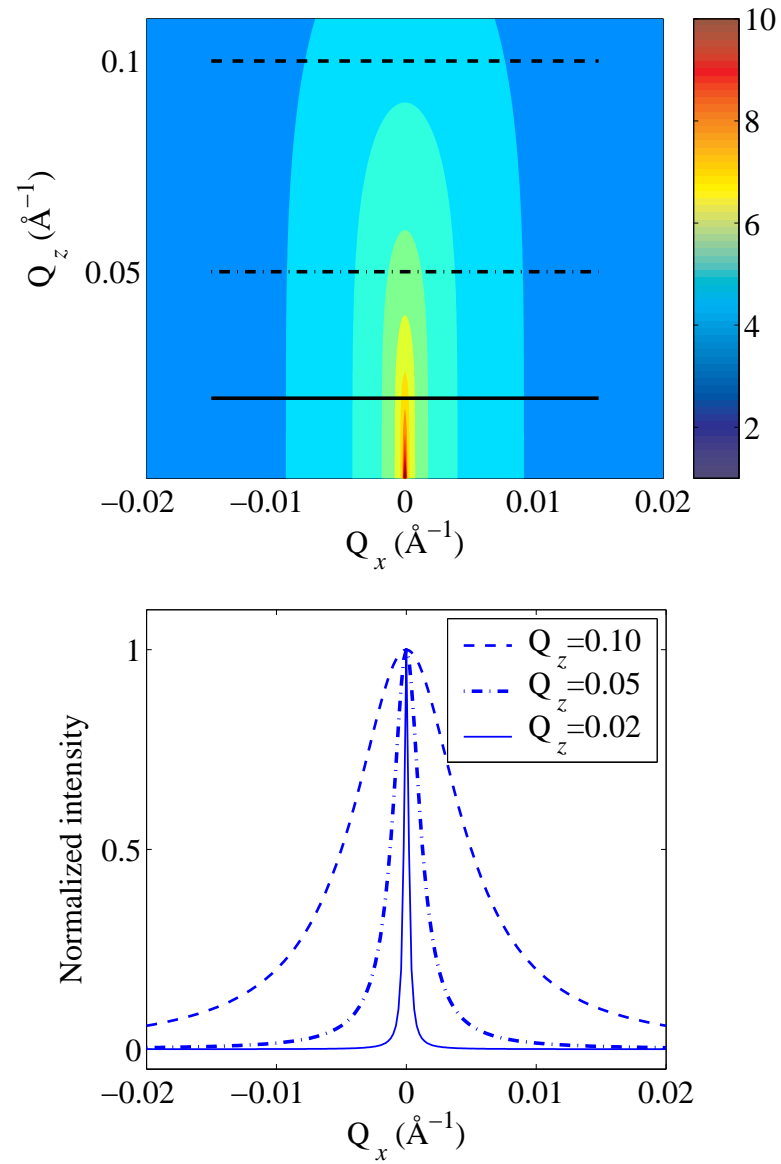


Figure 6: Simulation of non-specular reflectivity. Taken from Ref. [4]

3 Experimental considerations

Since the reflectivity falls off rapidly with Q_z , a high incident intensity is required for measurements up to relatively high Q_z . For laboratory sources typically one can detect reflectivities down to about 10^{-6} . At synchrotron sources, however, a larger dynamic range is accessible as well as the detection of the diffuse scattering to high angles.

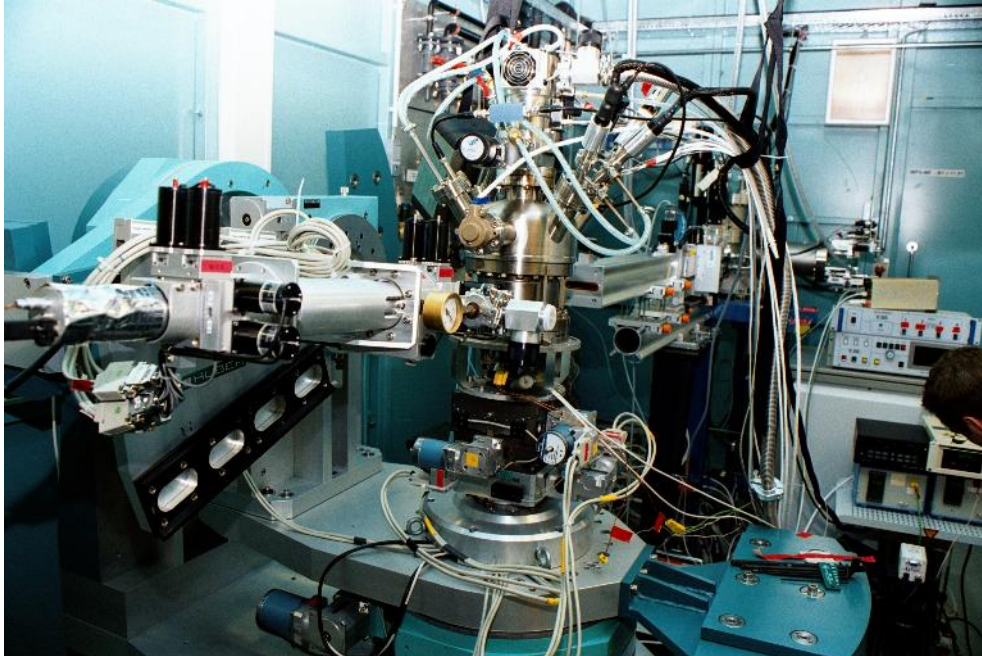


Figure 7: Experimental setup at a synchrotron source (ANKA, Karlsruhe)

References

- [1] M. Tolan, *X-Ray Scattering from Soft-Matter Thin Films*, Springer Tracts in Modern Physics, vol. 148 (Springer Heidelberg 1999)
- [2] F. Schreiber, *Structure and Growth of Self-Assembling Monolayers*, Prog. Surf. Sci. **65**, 151 (2000)
- [3] V. Holý, U. Pietsch, and T. Baumbach, *High-resolution x-ray scattering from thin films and multilayers*, Springer Tracts in Modern Physics, vol.149 (Springer, Berlin 1999)
- [4] J. Als-Nielsen and D. McMorrow, *Elements of Modern X-Ray Physics* (Wiley, Chichester, 2001)
- [5] T. P. Russell, *X-ray and neutron reflectivity for the investigation of polymers*, Materials Science Reports **5**, 171 (1990)
- [6] A. Baslau, P. S. Pershau, G. Swislow, B. M. Ocko, and J. Als-Nielsen, Phys. Rev. A **38**, 2457 (1988)

- [7] L. G. Parratt, *Surface studies of solids by total reflection of x-rays*, Phys. Rev. **95** 359 (1954)
- [8] P. Fenter, F. Schreiber, V. Bulovic, and S. R. Forrest, *Thermally induced failure mechanism of organic light emitting device structures probed by X-ray specular reflectivity*, Chem. Phys. Lett. **277**, 521 (1997)
- [9] I. W. Hamley and J. S. Pedersen, *Analysis of neutron and X-ray reflectivity*, J. Appl. Cryst. **27**, 29 (1994)
- [10] S. K. Sinha, E. B. Sinota, S. Garoff, and H. B. Stanley, *X-ray and neutron scattering from rough surfaces*, Phys. Rev. B **38**, 2297 (1988)